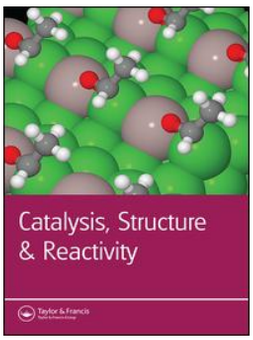

Catalysis, Structure & Reactivity

ISSN: 2055-074X (Print) 2055-0758 (Online) Journal homepage: http://www.tandfonline.com/loi/ycsr20

Understanding the role of promoters in catalysis: operando XAFS/DRIFTS study of $CeO_x/Pt/Al_2O_3$ during CO oxidation

E. K. Gibson, E. M. Crabb, D. Gianolio, A. E. Russell, D. Thompsett & P. P. Wells

To cite this article: E. K. Gibson, E. M. Crabb, D. Gianolio, A. E. Russell, D. Thompsett & P. P. Wells (2017) Understanding the role of promoters in catalysis: operando XAFS/DRIFTS study of $CeO_x/Pt/Al_2O_3$ during CO oxidation, Catalysis, Structure & Reactivity, 3:1-2, 5-12, DOI: 10.1080/2055074X.2017.1278890

To link to this article: http://dx.doi.org/10.1080/2055074X.2017.1278890

Published online: 14 Feb 2017.

CATALYSIS, STRUCTURE & REACTIVITY, 2017
VOL. 3, NO. 1–2, 5–12
http://dx.doi.org/10.1080/2055074X.2017.1278890

Taylor & Francis
Taylor & Francis Group

ORIGINAL RESEARCH PAPER

OPEN ACCESS

Understanding the role of promoters in catalysis: *operando* XAFS/DRIFTS study of $CeO_x/Pt/Al_2O_3$ during CO oxidation

E. K. Gibson[a,b], E. M. Crabb[c], D. Gianolio[d], A. E. Russell[e], D. Thompsett[f] and P. P. Wells[a,d,e]

[a]Rutherford Appleton Laboratory, UK Catalysis Hub, Research Complex at Harwell, Didcot, UK; [b]Department of Chemistry, University College London, London, UK; [c]Department of Life, Health and Chemical Sciences, The Open University, Milton Keynes, UK; [d]Diamond Light Source, Harwell Science and Innovation Campus, Didcot, UK; [e]School of Chemistry, University of Southampton, Southampton, UK; [f]Johnson Matthey Technology Centre, Blounts Court, Reading, UK

ABSTRACT

A combined *operando* XAFS/DRIFTS study on $CeO_x/Pt/Al_2O_3$ catalysts has been performed during CO oxidation and provides insights into the changes in nanoparticle structure and adsorbed species during the reaction profile. The onset of CO_2 formation is shown to be concurrent with a rapid re-oxidation of the Pt nanoparticles, evidenced by XAFS spectroscopy, and the loss of bridge bonded CO adsorbed on Pt, as shown by simultaneous DRIFTS acquisition. The continued appearance of linear bound CO on the catalyst surface is shown to remain long after catalytic light off. The interaction of Pt and CeO_x is evidenced by the improved performance towards CO oxidation, compared to the non-CeO_x modified Pt/Al_2O_3, and changes in the CO adsorption properties on Pt previously linked to Pt-CeO_2 interfaces.

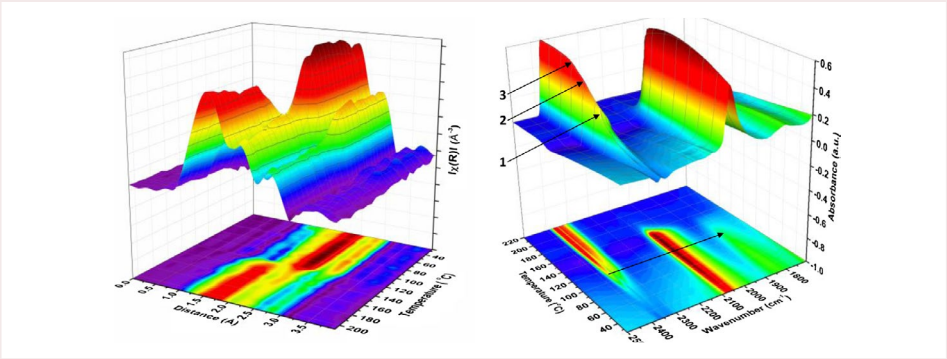

ARTICLE HISTORY
Received 26 September 2016
Accepted 30 November 2016

KEYWORDS
Operando; XAFS; DRIFTS; CO oxidation; Pt/Al_2O_3; catalysis; ceria

Introduction

The special interplay between metal nanoparticles and metal oxide supports is well-reported [1]. The role of the support is not only through the benign advantage of providing highly dispersed nanoparticles, instead it governs the structural morphology of the nanoparticles [2], alongside contributing additional active chemical species (e.g. redox centres [3]). One of the challenges of studying this relationship is the low number of atoms present at the interface between the nanoparticle and the metal oxide relative to that in the bulk of the particles. Wells et al. recently published work on the preparation of $CeO_x/Pt/Al_2O_3$ catalysts and their application for low temperature water gas shift (LTS) [4]. Here, a controlled amount of CeO_x was targeted at the Pt nanoparticles to maximise the relative interfacial area. The CeO_x is introduced onto preformed Pt/Al_2O_3 by the controlled surface reaction [5] between the reduced Pt with an organometallic precursor of Ce. LTS, along with reactions such as CO oxidation, are good model processes as the Al_2O_3 support has a far reduced impact on the performance of these reactions compared to CeO_2. The study showed that small amounts of CeO_x (0.35 wt%) were able to dramatically change the reaction profile, with Ce exhibiting facile redox switching from Ce^{3+} to Ce^{4+} at room temperature under reducing and oxidising atmospheres, respectively. This method has also been used elsewhere to improve the properties of Rh/Al_2O_3 catalysts for CO oxidation [6,7]. To understand these complex structure function relationships between metal nanoparticles and interfacial metal oxide clusters it is crucial to characterise the catalyst whilst it is operating under normal process conditions, this is to say, *operando*. X-ray absorption fine structure (XAFS) is an

CONTACT E. K. Gibson emma.gibson@rc-harwell.ac.uk; P. P. Wells ppwells@soton.ac.uk

ideal technique for probing metal nanoparticles using *operando* spectroscopy; the high intensity X-rays provided by a synchrotron (often of high energy depending on the absorption edge) are able to penetrate a range of sample environments [8,9], with XAFS not reliant on long range order to provide structural information. One limitation is the per atom average of the XAFS technique, which often fails to reflect the chemistry occurring at the surface of a catalyst, which is of course, where the catalysis happens. The combination of XAFS with surface sensitive techniques, such as diffuse reflectance infrared Fourier transform spectroscopy (DRIFTS), is able to provide a description of both the nanoparticle structure and the chemistry of the catalyst surface [10,11]. This study takes both approaches of controlled addition of promoters and combined spectroscopic techniques to assess the evolution of a $CeO_x/Pt/Al_2O_3$ catalyst during CO oxidation using simultaneous XAFS/DRIFTS acquisition.

Experimental

Catalyst preparation

Preparation of the $CeO_x/Pt/Al_2O_3$ catalyst has been reported elsewhere alongside its physicochemical characteristics [4]. In brief, 4 wt% Pt/ γ-Al_2O_3 supplied by Johnson Matthey was modified with CeO_x in a manner similar to that employed previously [5,12]. The Pt/ γ-Al_2O_3 was first reduced in flowing H_2(g) at 350 °C for 3 h and subsequently cooled to room temperature under flowing N_2(g). $Ce(acac)_3.H_2O$ was dissolved in toluene, purged with N_2(g) and added to the reactor. H_2(g) was then bubbled through the solution whilst stirring and heating at 90 °C for 8 h. Finally, the reactor was cooled and flushed with N_2(g) before the solid was collected and air dried. The initial reduction step was then repeated. The catalyst in this study was prepared with a Ce:Pt surface atomic ratio of 4:1.

Combined XAFS/DRIFTS

Pt L_3 edge XAFS studies were performed at the Diamond Light Source, UK, on beamline B18. Measurements were performed in transmission mode using ion chamber detectors with a fast scanning (QEXAFS) Si (1 1 1) double crystal monochromator. Each spectrum took 90 s to acquire (k_{max} = 14), with a Pt foil placed between I_t and $I_{ref.}$ Combined XAFS/DRIFTS studies were performed using a set-up based on that previous reported [13]. The experimental configuration involves a fast scanning FTIR spectrometer, equipped with a Harrick DaVinci arm, Praying Mantis optics, and a bespoke XAFS/DRIFTS reaction chamber, which was mounted on the experimental table (Figure 1(a)). The role of the DaVinci arm fitted with Praying Mantis optics was to refocus the beam onto the top of the sample external to the FTIR

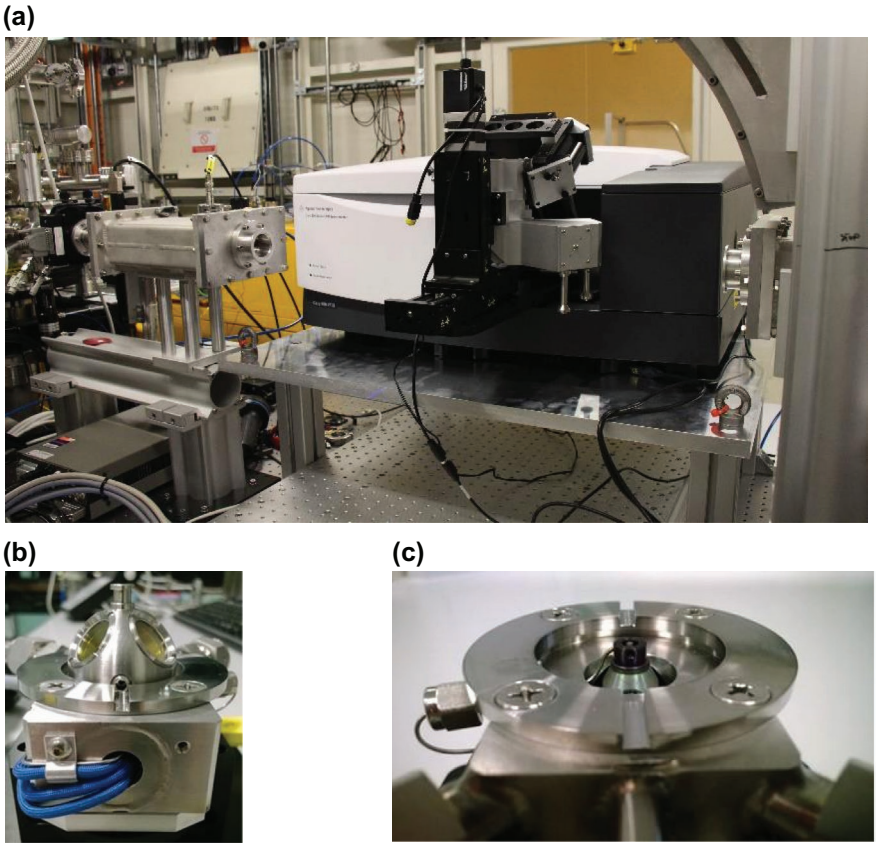

Figure 1. (a) Combined XAFS/DRIFTS system mounted on the beamline, B18 at Diamond Light Source, (b) external view on reaction chamber, and (c) internal view of reaction cahmber.

spectrometer, to allow X-rays to pass through the reaction chamber, whilst maintaining a purged (N_2) environment. The DaVinci arm was fitted with stepper motors to facilitate precise alignment with the X-ray beam, which provided movement in vertical and horizontal directions of 48 mm. The reaction chamber (Figure 1(b)), which has been described in detail elsewhere [13], is based on a conventional dome based Harrick high temperature and pressure reaction chamber fitted with ZnSe windows for the collection of DRIFTS data and glassy carbon windows for entry and exit of the X-ray beam. The sample cup (Figure 1(c)) has a diameter of 3 mm and is fitted with holes for the X-ray beam to pass through. The top of these holes are 0.37 mm from the surface of the catalyst bed. At this distance assuming an IR penetration depth in of ~1–2 mm [14], the X-rays and IR beams should be sampling the same region of the catalyst bed [15]. The cell has a total dead volume of 14 ml, making it non ideal for kinetic measurements, therefore, no direct comparison of activity results are made between the XAFS/DRIFTS study and those of the fixed bed reactor. DRIFTS spectra were acquired with an Agilent Carey 680 FTIR spectrometer (64 scans, resolution 4 cm^{-1}) using a liquid nitrogen cooled MCT detector. CO oxidation experiments were carried out using a 1:1 ratio of 10% CO/He and 10% O_2/He over approximately 129 mg of catalyst, the total flow was 25 mL/min, the space velocity in the reactor was 11628 $cm^3\ g^{-1}\ h^{-1}$. XAFS/DRIFTS data was first collected under He at room temperature before the introduction of reactant gases. The temperature was increased at a steady ramp rate of 3 °C min^{-1}, until a maximum temperature of 220 °C was achieved. Outlet gases were sample continuously with an online MKS mass spectrometer. During reaction XAFS and DRIFTS spectra were sampled continuously with a time resolution of 90 s and 30 s, respectively.

CO oxidation testing

CO oxidation testing was carried out using a fixed bed reactor; 0.2 g of pelletised catalyst was loaded into the reactor tube on a bed of glass wool, ensuring the thermocouple was in the catalyst bed layer. The inlet gases were a mixture of N_2, 1% CO in N_2, and air with a total flow of 300 $cm^3\ min^{-1}$, the space velocity in the reactor was 90000 $cm^3\ g^{-1}\ h^{-1}$. The flow of air was kept constant and the flows of N_2 and CO were adjusted to control the mole fraction of CO. The temperature was ramped manually, the procedure involved simultaneously heating the furnace and cooling with liquid nitrogen to facilitate a very slow heating rate and combat the exothermic reaction conditions. The gas analysis was performed using a Maihak s710 analyzer comprising of a H_2 detector and IR CO and CO_2 sensors. Three thermocouples are placed inside the reactor chamber to monitor the temperature of the gas inlet, gas outlet and the catalyst bed.

Results

The physicochemical properties of the $CeO_x/Pt/Al_2O_3$ catalyst have been reported elsewhere [4]. In brief, the catalyst was found to have Ce and Pt content of 2.3 and 3.8 wt%, respectively by ICP-OES analysis. Transmission electron microscopy identified Pt nanoparticles <2 nm, however, dense agglomeration prevented an accurate assessment of the particle size distribution. Ce L_3 XANES studies showed mixed valence Ce (Ce^{3+} and Ce^{4+}) at room temperature under an atmosphere of air, progressing to complete reduction to Ce^{3+} under atmospheres of H_2 and CO. This facile reduction properties of Ce at room temperature served as evidence of the co-locality of Ce and Pt.

Prior to applying the temperature ramp in the XAFS/DRIFTS reaction chamber under the CO and O_2 gas mixture, XAFS spectra were recorded at room temperature before and after the introduction of reactant gases. The comparison of these two states is highlighted by assessing the X-ray absorption near edge structure (XANES), as seen in Figure 2, and the extended X-ray absorption fine structure (EXAFS), as seen in Figure 3. Both sets of data provide evidence for an initial catalyst that is highly oxidised; the XANES shows an intense white line and the EXAFS is dominated by a primary scattering path associated with Pt-O (non phase-corrected position of 1.6 Å). The Pt–Pt features in the EXAFS data are consistent with Pt^0, and confirm that initially Pt is present as small metal nanoparticles with an oxidic skin. There is no evidence of longer oxygen bridged Pt–Pt distances, characteristic of PtO. On addition of the reactant gas mixture the intensity of the white line is reduced, as is the feature in the Fourier transform indicative of Pt-O. This shows that despite the excess of O_2, CO acts as an able reductant and the surface oxide is removed.

The Pt reduction under CO:O_2 at room temperature was allowed to stabilise, before the temperature ramp was applied. The time resolved *operando* XANES and EXAFS (k^2 Fourier transform) data during CO oxidation are shown in Figures 4 and 5, respectively.

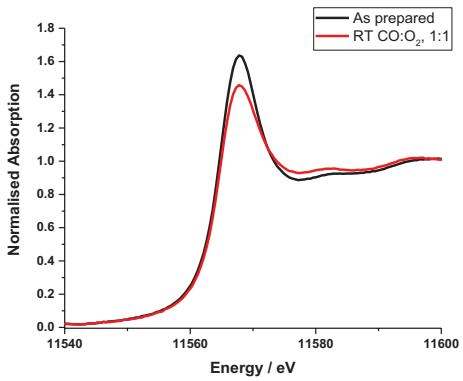

Figure 2. Normalised XANES spectra of $CeO_x/Pt/Al_2O_3$ in air and a 1:1 mixture of 10% CO/He and 10% O_2/He.

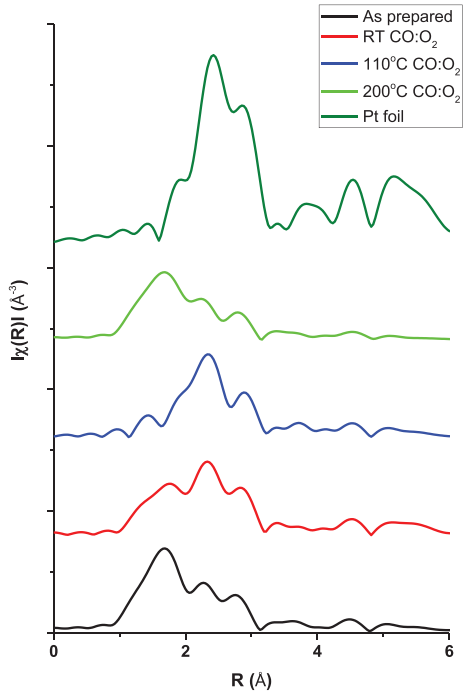

Figure 3. Non phase-corrected k^2 weighted Fourier transform EXAFS data of $CeO_x/Pt/Al_2O_3$ in air and a 1:1 mixture of 10% CO/He and 10% O_2/He at room temperature, 110, 200 °C. A Pt foil is included for comparison.

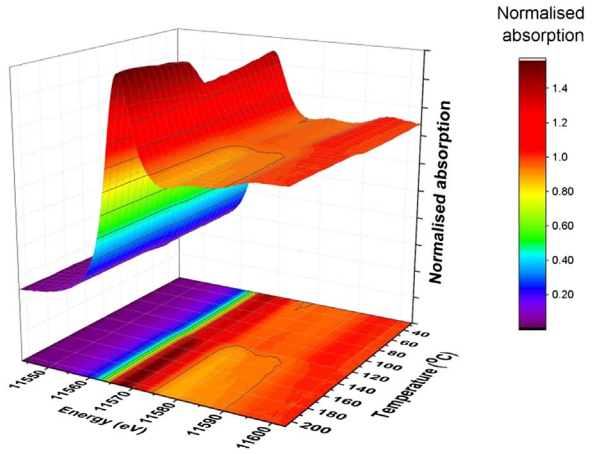

Figure 4. *Operando* XANES data of $CeO_x/Pt/Al_2O_3$ during CO oxidation conditions.

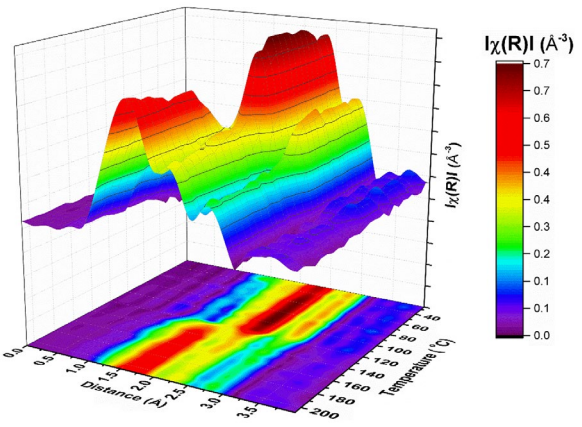

Figure 5. *Operando* EXAFS data of $CeO_x/Pt/Al_2O_3$ during CO oxidation conditions.

The XANES data show that the onset of the increased temperature was accompanied by a further gradual reduction of Pt, before a sharp re-oxidation between 120 and 130 °C. This can be rationalised as the temperature at which catalytic 'light off' occurs. After this point the CO has been completely oxidised to CO_2, which will be assessed by the online mass spectrometry and DRIFTS spectra in the following section, and the gas environment returns to net oxidising conditions. The initial reduction of white line intensity on increasing the temperature, observed in the XANES, correlates with a reduction in the region of the Fourier transform (non phase-corrected distance ~1.6 Å) associated with Pt-O scattering paths, however, the effect is less pronounced. Immediately prior to light off the EXAFS is consistent with entirely metallic Pt with no Pt–O interactions, this is highlighted by a comparison of this state with a Pt foil reference spectrum (Figure 3). Fitting the EXAFS data (Table 1) of this reduced state of Pt, provides a primary Pt–Pt coordination number of 10 (±1), which when applying the method of Beale et al. [16], can be used to deduce an average particle size of 2.4 nm. In this instance only the 1st shell contributions have been included in the fitting analysis as this adequate for determining the extent of oxidation, and in the case of the purely metallic system the particle size determination.

An investigation by van Bokhoven and co-workers looked at a Pt/Al_2O_3 catalyst under similar CO oxidation conditions using XAFS [17]. Their study showed similar trends and highlighted that the Pt–Pt bond distance, contracted after light off as a consequence of surface relaxation by adsorbed CO. We also observe this change in distance (Table 1) between the reduced form of Pt and that post light off. However, the Pt–Pt distance post light off, is the same as the initial catalyst (within error), prior to CO exposure. Indeed, we find the Pt–Pt distance similar to that of other surface oxidised Pt nanoparticles reported elsewhere in the literature [18]. This observation is consistent with the fact that post light off the surface coverage is significantly oxygen rich as CO is continually being converted to CO_2. Another difference with this study is the temperature of light off, which occurs ~60 °C higher than we report here. Indeed, to assess the effect of CeO_x the modified Pt/Al_2O_3 and reference samples were tested using a fixed bed reactor set-up (Figure 6). The conditions were different to that used in the combined XAFS/DRIFTS study, and

Table 1. EXAFS fitting parameters of $CeO_x/Pt/Al_2O_3$.

Condition	Abs. Sc.	*N*	*R*/Å	$2\sigma^2$/Å^2	E_0/eV	R_{factor}
As prepared	Pt–O	2.4 (4)	2.01 (2)	0.005 (2)	10 (2)	0.01
	Pt–Pt	4(2)	2.74 (1)	0.007 (3)		
110 °C CO:O_2	Pt–Pt	10 (1)	2.76 (1)	0.011 (1)	7(1)	0.02
200 °C CO:O_2	Pt–O	1.8 (3)	2.00 (1)	0.005 (2)	7(2)	0.007
	Pt–Pt	6 (2)	2.73 (2)	0.011 (2)		

Note: Fitting parameters: $S_0^2 = 0.85$; Fit range $3.1 < k < 11$, $1.1 < R < 3$; # of independent points = 9.

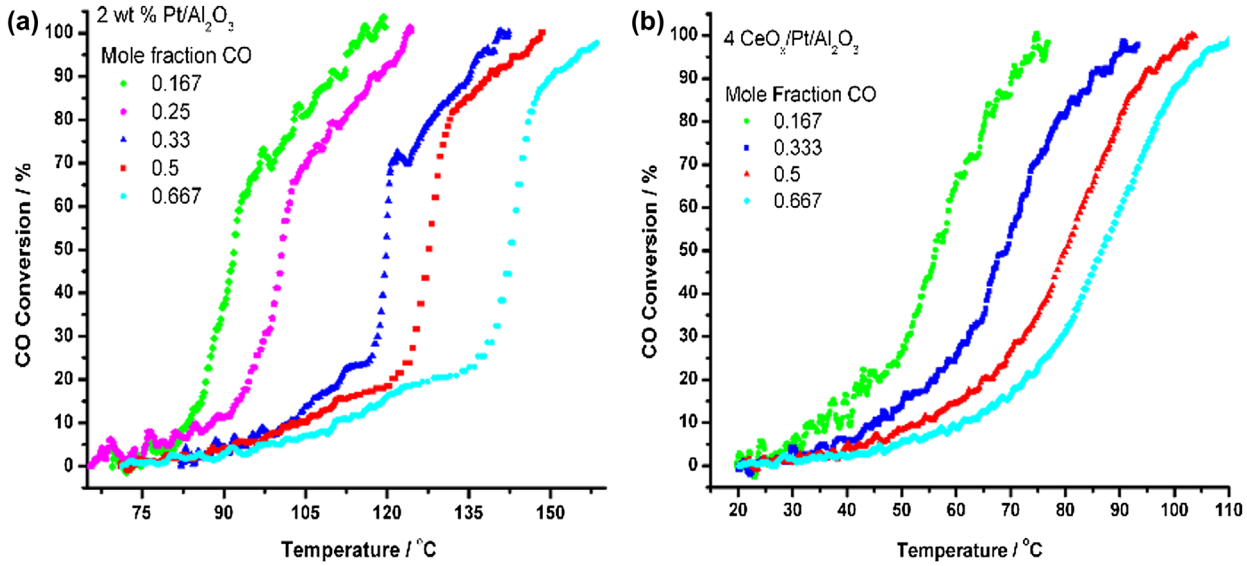

Figure 6. CO oxidation testing of (a) Pt/Al_2O_3, and (b) $CeO_x/Pt/Al_2O_3$.

therefore report different values for CO oxidation performance, as we wished to assess the reaction rate order with respect to CO.

Figures 6(a) shows the CO conversion plot for Pt/Al_2O_3. It can be seen that the plot shows a characteristic light off feature, where there is a sharp increase in the conversion of CO. As a steep light-off curve is not observed for the $CeO_x/Pt/Al_2O_3$ catalyst, the light-off temperature is defined here as the temperature at which 50% CO conversion (T_{50}) was obtained. $CeO_x/Pt/Al_2O_3$ (Figure 6(b)) is the more active catalyst and has a T_{50} value (Table 2) of 69 °C for X_{CO} = 0.33. This compares to the value of 120 °C for Pt/Al_2O_3. Moreover, the CO conversion plot for the $CeO_x/Pt/Al_2O_3$ has different features to that of Pt/Al_2O_3; there is a more gradual increase in CO conversion with increasing temperature than the intense light off feature associated with Pt/Al_2O_3.

The CO oxidation reaction was also assessed during the combined XAFS/DRIFTS study with the mass spectrometry results shown in Figure 7. Three rates of CO_2 production are observed during the temperature ramp, a gradual increase from 100° with a step at 117 °C, followed by a more gradual increase up to ~143 °C, after which the rate of CO_2 production slows until 220 °C (75 min), at which point the temperature was maintained at 220 °C. The first sharp increase and the second faster CO_2 production rate are consistent with the XAFS results which showed a fast re-oxidation of Pt between 120–130 °C.

The simultaneous DRIFTS study allows us to follow changes in Pt speciation by assessing changes in CO

Table 2. Temperature at which 50% CO conversion was attained (T_{50}) for the CO oxidation testing at different mole fractions of CO for different catalysts.

Catalyst	T_{50} at different values of X_{CO}/°C			
	X_{CO} = 0.167 %CO = 0.8 CO:O_2 = 1:53	X_{CO} = 0.33 %CO = 0.17 CO:O_2 = 1:25	X_{CO} = 0.5 %CO = 0.25 CO:O_2 = 1:17	X_{CO} = 0.667 %CO = 0.33 CO:O_2 = 1:13
Pt/Al_2O_3	92	120	128	143
$CeO_x/Pt/Al_2O_3$	56	69	80	87

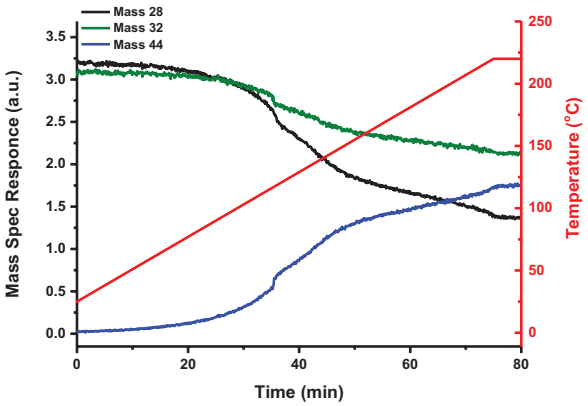

Figure 7. Mass spectrometer response during temperature ramp, (3 °C min^{-1}) showing traces of masses 18, 28, 32 and 44 representing H_2O, CO (and CO_2), O_2 and CO_2 respectively. The temperature profile is shown in red.

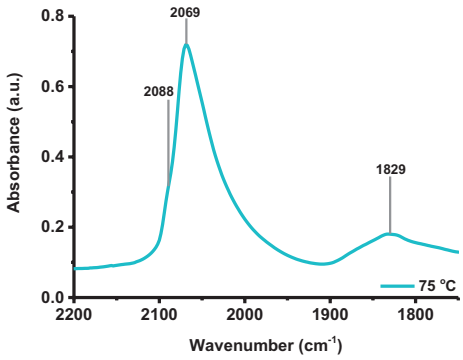

Figure 8. DRIFTS spectra collected during CO oxidation XAFS/DRIFTS experiment at 75 °C.

binding modes on the Pt surface. One example of this is the intense linear bound CO adsorption bands centred ~2070 cm^{-1}, shown in Figure 8. This band has a shoulder at 2087 cm^{-1} and a broad tail towards lower wavenumbers, ~2020 cm^{-1}. These linearly bound CO adsorption bands are very similar to those observed in the literature for CO adsorbed on Pt-CeO_2/Al_2O_3 catalysts, with the intense band at 2070 cm^{-1}assigned to CO adsorbed on steps or corners of Pt particles, and the shoulder at 2088 cm^{-1} being attributed to CO linearly adsorbed on Pt with a neighbouring Pt atom containing adsorbed O [19,20]. Both of these bands shift to lower wavenumber during reaction, at 25 °C they appear at 2091 and 2070 cm^{-1} shifting to 2088 and 2062 cm^{-1} respectively, by 150 °C. Which is consistent with a loss in vibrational coupling between the CO molecules which occurs at high coverage [21,22]. The broad tail at ~2020 cm^{-1} may provide evidence of the close proximity of the Pt and CeO_2, as this band has been previously assigned to CO adsorbed on Pt interacting with CeO_2 and similarly for Rh/CeO_2 samples where it was assigned to CO adsorbed on Rh atoms at the metal-support interface [20,23,24].

A 3D plot of the evolution of the gas phase CO_2 bands and CO adsorption bands with temperature during the CO oxidation ramp is shown in Figure 9. In agreement with the mass spectrometry data, three regions of CO_2 production are observed. The gas phase CO_2 bands, observed between 2395-2273 cm^{-1}, increase sharply at 110–120 °C, then more gradually up to 150 °C, with the third slower rate of production observed from 150 to 220 °C. The integration of the CO_2 region compared to the CO conversion is shown in Figure 10. Linearly adsorbed CO on metallic Pt, the band centred at 2071 cm^{-1}, reaches a maximum intensity at ~120 °C, notably this is after the reaction light-off. The linear adsorbed CO decreases gradually during the second CO_2 production region, from 120 to 155 °C before desorbing suddenly at 160 °C, and consistent with a decrease in CO coverage, this band shifts to lower wavenumber during reaction. The initial fast CO_2 production rate from 110 to 120 °C coincides with the disappearance of the broad band centred at 1829 cm^{-1}, which is consistent with CO bridge bonded to metallic Pt sites [20]. Correlating these changes in CO adsorption bands with the CO_2 production temperatures, we propose that the bridge bonded CO species are most likely involved in the fast CO_2 production at 110–120 °C and the linear bound CO species on corner sites, ~2069 cm^{-1}, are associated with the second and third slower regions of CO_2 production. The comparison of the steep decrease in bridged CO species coincident with the first sharp increase in CO conversion, can be more clearly observed from the integrated intensities of the IR bands compared with the CO conversion in Figure 10. Our observation of strongly bound linearly adsorbed CO species, resisting desorption or reaction above significant conversion, differs to literature reports of CO oxidation over Pt/Al_2O_3 and $Pt/CeO_2–Al_2O_3$ [25]. In this literature study the linearly adsorbed CO correlates directly with CO_2 production. However, our approach of applying multiple spectroscopic probes allows us to understand this process in greater detail.

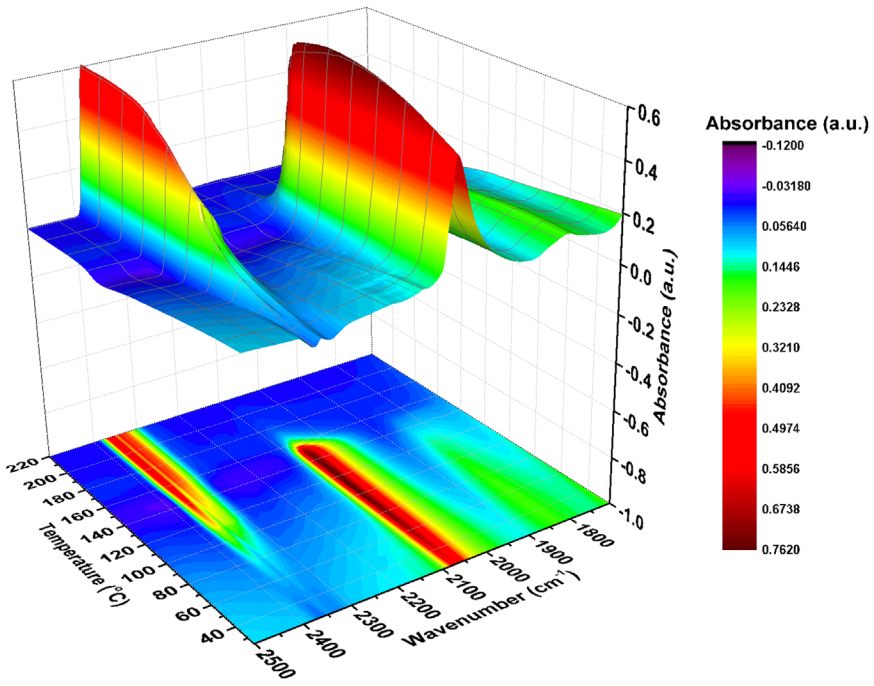

Figure 9. 3D plot of the DRIFTS spectra collected during CO oxidation XAFS/DRIFTS experiment. The numbers, 1,2,3 refer to the CO_2 production regions, and the arrow on the bottom projection of band intensities highlights the correlation between the bridged bonded CO band at 1829 cm^{-1} and the initial increase in the CO_2 bands.

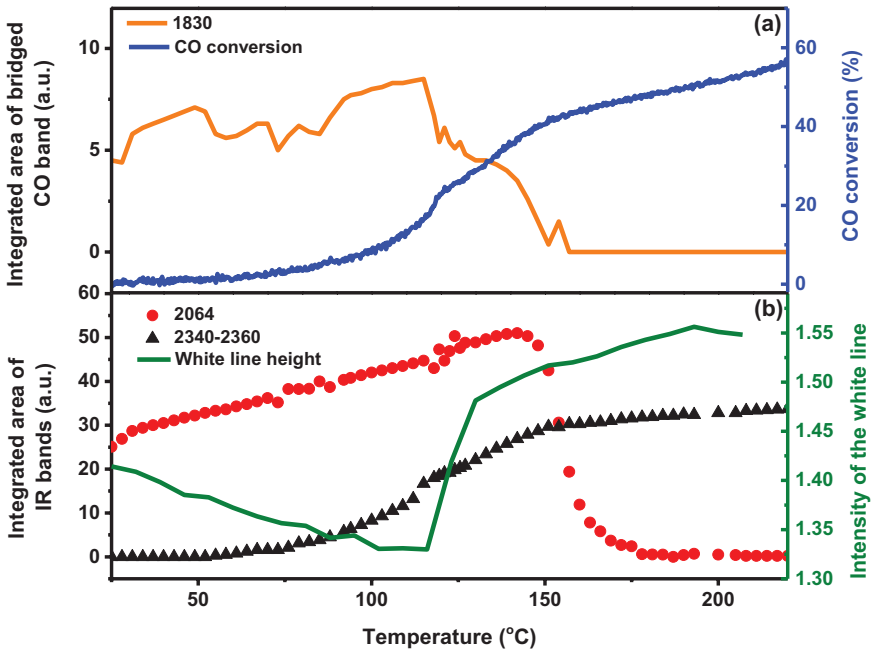

Figure 10. Integrated area of IR (a) CO band compared to the CO conversion and (b) comparison of the integrated band area of linear CO band (2064 cm^{-1}), CO_2 (2340–2360 cm^{-1}) compared to the intensity of the white line from the XAFS data.

Conclusion

The combined *operando* XAFS/DRIFTS study of a $CeO_x/Pt/Al_2O_3$ catalyst during CO oxidation reported here shows how catalytic properties can be dramatically altered by small addition of promoters, in this case CeO_x. Our testing data shows that the addition of CeO_x increases the performance towards CO oxidation by changing the reaction rate order with respect to CO. We also show that significant conversion of CO to CO_2, is achieved through the loss of bridge bonded CO adsorbed on Pt. Indeed, there is relatively little change in CO conversion after the linearly adsorbed CO is removed ~40 °C later. Moreover, the loss of bridge-bonded CO is concurrent with the rapid re-oxidation of Pt NPs, as evidenced by the time resolved XAFS studies. There is slight increase in white line intensity around 160 °C, however it essentially negligible compared to the rapid change observed at 120 °C, shown in Figure 10. This confirms that the majority of Pt sites are involved in bridge bonding of CO and why the activity, with regards to CO_2 production, is linked to the loss of these species in the DRIFTS spectra. Further evidence of the Pt–CeO_x interaction is shown through changes in the shape of the linearly bound CO adsorption band, where a clear tailing is observed and has been previously been linked to Pt–CeO_2 interfaces. *In fine*, the study shows that by preparing model materials and performing combined *operando* spectroscopy we are able to correlate both changes in NP properties and adsorbed surface species with the reaction profile.

Acknowledgements

EKG and PPW wish to thank Diamond Light Source and the UK Catalysis Hub block allocation award for beamtime (SP8071). Diamond Light Source are also thanked for the outstanding support of the staff on B18: Prof. Andrew Dent, Dr Giannantonio Cibin, Dr Stephen Parry and Mr Phil Robbins. The access to equipment provided by the Diamond industrial liaison team is gratefully acknowledged. Dr Khaled Mohammed, Dr Michal Perdjon, Anna Kroner and Anna Gould are thanked for assistance in collecting the data. The UK Catalysis Hub is kindly thanked for resources and support provided via our membership of the UK Catalysis Hub Consortium and funded b EPSRC (portfolio grants EP/K014706/1, EP/K014668/1, EP/K014854/1, EP/K014714/1 and EP/I019693/1). The EPSRC are also thanked for the strategic equipment grant for the combined XAFS/DRIFTS set-up (EP/K005030/1). Johnson Matthey are thanked for financial support and provision of materials.

Disclosure statement

No potential conflict of interest was reported by the authors.

Funding

This work was supported by the Engineering and Physical Sciences Research Council (EPSRC) [grant number EP/K014706/1], [grant number EP/K014668/1], [grant number EP/K014854/1], [grant number EP/K014714/1], [grant number EP/I019693/1], and [grant number EP/K005030/1].

ORCID

E. K. Gibson http://orcid.org/0000-0002-7839-3786
P. P. Wells http://orcid.org/0000-0002-0859-9172

References

[1] Evans J, Newton MA. Towards a structure-activity relationship for oxide supported metals. J Mol Catal A-Chem. 2002;182–183:351–357.

[2] Farmer JA, Campbell CT. Ceria maintains smaller metal catalyst particles by strong metal-support bonding. Science. 2010;329:933–936.

[3] Meunier FC, Tibiletti D, Goguet A, et al. On the complexity of the water-gas shift reaction mechanism over a Pt/CeO_2 catalyst: effect of the temperature on the reactivity of formate surface species studied by operando DRIFT during isotopic transient at chemical steady-state. Catal Today. 2007;126:143–147.

[4] Wells PP, Crabb EM, King CR, et al. Reduction properties of Ce in $CeO_x/Pt/Al_2O_3$ catalysts. Catal Struct React. 2015;1:88–94.

[5] Wells PP, Crabb EM, King CR, et al. Preparation, structure, and stability of Pt and Pd monolayer modified Pd and Pt electrocatalysts. Phys Chem Chem Phys. 2009;11:5773–5781.

[6] Kroner AB, Newton MA, Tromp M, et al. Structural characterization of alumina-supported Rh catalysts: effects of ceriation and zirconiation by using metal-organic precursors. Chem Phys Chem. 2013;14:3606–3617.

[7] Kroner AB, Newton MA, Tromp M, et al. Time-resolved, *in situ* DRIFTS/EDE/MS studies on alumina-supported rhodium catalysts: effects of ceriation and zirconiation on Rhodium–CO interactions. Chem Phys Chem. 2014;15:3049–3059.

[8] Bartlett SA, Wells PP, Nachtegaal M, et al. Insights in the mechanism of selective olefin oligomerisation catalysis using stopped-flow freeze-quench techniques: a Mo K-edge QEXAFS study. J Catal. 2011;284:247–258.

[9] Wiltshire RJK, King CR, Rose A, et al. A PEM fuel cell for *in situ* XAS studies. Electrochim Acta. 2005;50:5208–5217.

[10] Rogers SM, Catlow CRA, Chan-Thaw CE, et al. Tailoring gold nanoparticle characteristics and the impact on aqueous-phase oxidation of glycerol. Acs Catal. 2015;5:4377–4384.

[11] Newton MA, Burnaby DG, Dent AJ, et al. Energy dispersive extended X-ray absorption fine structure, mass spectrometric, and diffuse reflectance infrared studies of the interaction of Al_2O_3-supported $Rh\text{-}I(CO)_2Cl$ species with NO and re-formation under CO. J Phys Chem B. 2002;106:4214–4222.

[12] Wells PP, Qian Y, King CR, et al. To alloy or not to alloy? Cr modified Pt/C cathode catalysts for PEM fuel cells. Faraday Discuss. 2008;138:273–285.

[13] Marinkovic NS, Wang Q, Frenkel AI. *In situ* diffuse reflectance IR spectroscopy and X-ray absorption spectroscopy for fast catalytic processes. J Synchrotron Radiat. 2011;18:447–455.

[14] Highfield JG, Prairie M, Renken A. *In-situ* drift spectroscopy in a continuous recycle reactor – a versatile tool for catalytic process research. Catal Today. 1991;9:39–46.

[15] Marinkovic NS, Wang Q, Barrio L, et al. Combined *in situ* X-ray absorption and diffuse reflectance infrared spectroscopy: an attractive tool for catalytic investigations. Nucl Instrum Methods Phys Res Sect A-Accel Spectrom Dect Assoc Equip. 2011;649:204–206.

[16] Beale AM, Weckhuysen BM. Phys Chem Chem Phys. EXAFS as a tool to interrogate the size and shape of mono and bimetallic catalyst nanoparticles. 2010;12:5562–5574.

[17] Alayon EMC, Singh J, Nachtegaal M, et al. In: DiCicco A, Filipponi A, editors. 14th International Conference on X-ray Absorption Fine Structure; 2009, vol. 190; Bristol: Iop Publishing Ltd.

[18] Martinelli M, Jacobs G, Graham UM, et al. Water-gas shift: characterization and testing of nanoscale YSZ supported Pt catalysts. Appl Catal A-Gen. 2015;497:184–197.

[19] Jin T, Zhou Y, Mains GJ, et al. Water-gas shift: characterization and testing of nanoscale YSZ supported Pt catalysts. J Phys Chem. 1987;91:5931–5937.

[20] Martínez-Arias A, Coronado JM, Cataluña R, et al. Influence of mutual platinum-dispersed ceria interactions on the promoting effect of ceria for the CO oxidation reaction in a $Pt/CeO_2/Al_2O_3$ catalyst. J Phys Chem B. 1998;102:4357–4365.

[21] Ferri D, Bürgi T, Baiker A. Pt and Pt/Al_2O_3 thin films for investigation of catalytic solid-liquid interfaces by ATR-IR spectroscopy: CO adsorption, H-2-induced reconstruction and surface-enhanced absorption. J Phys Chem B. 2001;105:3187–3195.

[22] Sheppard N, Nguyen TT. In: Clark RJH, Hester RE. Advances in infrared and Raman spectroscopy. London: Heyden & Son; 1978, vol. 5; p. 67–148.

[23] Bensalem A, Muller J-C, Tessier D, et al. Spectroscopic study of CO adsorption on palladium-ceria catalysts. J Chem Soc Faraday Trans. 1996;92:3233–3237.

[24] Soria J, Martinez-Arias A, Fierro JLG, et al. Vacuum. Effect of outgassing treatments on the surface reactivity of Rh/CeO, catalysts: CO adsorption. 1995;46:1201–1204.

[25] Daniel C, Clarté M-O, Teh S-P, et al. Spatially resolved catalysis in microstructured reactors by IR spectroscopy: CO oxidation over mono- and bifunctional Pt catalysts. J Catal. 2010;272:55–64.